

Investigation of a NACA0012 Finite Wing Aerodynamics at Low Reynold's Numbers and 0° to 90° Angle of Attack

Shahrooz Eftekhari^{1*}, Abdulkareem Shafiq Mahdi Al-Obaidi¹

Eftekhari S  <https://orcid.org/0000-0003-3855-3826>
Al-Obaidi ASM  <https://orcid.org/0000-0003-2575-0441>

How to cite

Eftekhari S, Al-Obaidi ASM (2019) Investigation of a NACA0012 Finite Wing Aerodynamics at Low Reynold's Numbers and 0° to 90° Angle of Attack. J Aerosp Technol Manag, 11: e1519. <https://doi.org/10.5028/jatm.v11.1023>

ABSTRACT: The aerodynamic characteristics of a NACA0012 wing geometry at low Reynold's numbers and angle of attack ranging from 0° to 90° are investigated using numerical simulations and the results are validated by wind tunnel experiments. Further experiments are conducted at low Reynold's numbers of 1×10^5 , 2×10^5 and 3×10^5 . Findings of the study show a similar trend for the lift and drag coefficients at all the investigated Reynold's numbers. The lift coefficient is linearly increased with angle of attack until it reaches its maximum value at 32° which is the stall angle. It is observed that further increment in angle of attack results in decrement of lift coefficient until it reaches its minimum value at 90° angle of attack. The drag force acting on the airfoil increases as the angle of attack is increased and increment in the drag force results in change of laminar flow to turbulent flow. As the turbulence gets higher the flow starts to separate from the airfoil surface due to eddies generated by turbulence. Hence, the lift force generated by the wing is reduced and drag force is increased simultaneously, which results in poor performance of the wing.

KEYWORDS: NACA0012, Finite wing, Aerodynamic characteristics, High angle of attack, Low Reynold's number.

INTRODUCTION

Throughout the past century, researches and developments have been conducted on wings, which contributes to a constructive role in designing wind turbines, ship rudder, missiles and aviation industries. NACA0012 is a well-known airfoil that is utilized in academic researches as well as industrial applications such as Mini-Unmanned Aerial Vehicle (MUAV) (Kim *et al.* 2011). The MUAVs fly at low velocity and small length scale that put them in low wing chord Reynolds number flight regime ranging from 1.5×10^4 to 5×10^5 , which is below that of conventional aircrafts (Chahl 2015). The aerodynamic performance of MUAVs is critically dependent on the lifting surface, i.e. the wing.

Ahmed *et al.* (2014) numerically examined the behavior of lift and drag coefficients of NACA0012 at 0° to 50° angle of attack using a $k - \omega$ shear stress transport (SST) turbulence model. The number of nodes was increased to reach a cell number of 120000 to have a satisfactory mesh size and accurate results. The obtained results at 0°, 10° and 15° angle of attack were then compared with NASA's Langley Research Centre Validation Case for validation (Abbott and Von Doenhoff 1959). The results show that for a Mach number of 0.2 and 10° angle of attack, the lift and drag coefficients

¹Taylor's University – Innovation and Technology – Engineering – Petaling Jaya/Selangor – Malaysia.

*Correspondence author: shahroozeftekhari@sd.taylors.edu.my

Received: Jan. 30, 2018 | Accepted: Jun. 27, 2018

Section Editor: Rho Shin Myong



are 0.019 and 0.001, respectively. On the other hand, by increasing the angle of attack to 50° , the lift coefficient drops to 0.015, while the drag coefficient increases to 0.006. In another study, Zhang *et al* (2010) numerically studied the flow field of NACA0012 at 0° to 180° using C-type grid with 360 cells, H-type grid with 200 cells and O-type grid with 320 cells. The Mach number and Reynold's number were set to 0.15 and 0.5×10^6 , respectively. The simulation was performed for angle of attack ranging from 10° to 70° utilizing Spalart-Allmaras, standard $k - \epsilon$, RNG $k - \epsilon$, as well as SST $k - \omega$ turbulent model. The simulations were conducted for 0° to 180° angle of attack on the NACA0012 utilizing Spalart-Allmaras turbulence model. Comparison of the numerical for different grid topologies shows that C-type grid has the best fit to the experimental results while coefficients obtained from the H-type and O-type grid show a great scatter at angle of attack. Hence the C-type grid was found to be a more reliable grid type, compared to O-type and H-type.

Windi *et al.* (2014) conducted a 2-D numerical analysis on the flow separation around NACA0012 at different angles of attack ranging from 0° to 20° {Imad shukri, 2011 #17}{Imad shukri, 2011 #17} using the $k - \epsilon$ turbulent model. The results from the analysis show that increasing the angle of attack results in significant separation of the flow. The flow is observed to be laminar below 10° angle of attack. From 0° to 10° angle of attack there is no separation and lift coefficient increases while the drag coefficient is nearly constant. Increments after 10° result in increase of adverse pressure gradient on the upper surface, which causes turbulence. It was also found that the lift coefficient increases until 12° angle of attack without significant change in drag coefficient and the separation happens at the tail of the airfoil. The separation continues growing until a critical angle of attack (stall angle) of 15° , in which the flow is fully separated from the upper surface of airfoil and the lift coefficient increases slowly while the drag coefficient increases dramatically.

An experimental study was conducted by Zhou *et al.* (2011) to measure the mean forces acting on NACA0012 at angle of attack ranging from 0° to 90° and low Reynolds number of 5.3×10^3 and 5.1×10^4 using a closed loop water tunnel. The results were then compared with Devinant *et al.* (2002) test data for 0° to 90° angle of attack. The experimental results show that the lift coefficient increases as the angle of attack increases from 0° to 15° . Further increments of angle of attack result in decrements in lift coefficient until it reaches 0.1 at 90° angle of attack. However, the increments of drag coefficient are linear and relatively small for angle of attack less than 15° , and it starts to have a sudden increment at 15° angle of attack until it reaches 2.1 at 90° .

Previous studies have examined the aerodynamics of NACA0012 airfoils and wings at different angles of attack. However, the available data for finite wing aerodynamic characteristics at low Reynold's numbers are limited. The aim of this study is to provide a better understanding of the aerodynamic characteristics of a finite NACA0012 wing at angles of attack ranging from 0° to 90° and Reynold's number of 1×10^5 , 1.29×10^5 , 2×10^5 , and 3×10^5 . The findings of the study enable aeronautical industries to have a detailed understating of the flow behavior at such low speed flight regime.

NUMERICAL SIMULATION

Numerical simulations have recently developed a good reputation in engineering researches. One of the applicable numerical methods is the computational fluid dynamics (CFD) (Chung 2002). Computer software has been utilized CFD in the research methodology to expedite the research process and to reduce the cost of prototypes and experiments. In order to achieve reliable results through simulation process, it is important to apply the right meshing method and boundary conditions. The numerical simulations in this paper are conducted using ANSYS FLUENT 15.0.

WING GEOMETRY AND FLUID DOMAIN

A fluid domain is generated around a rectangular NACA0012 wing geometry with aspect ratio of 1 (Fig. 1). The C-Type grid topology is used to generate the mesh around the wing and domain boundaries are located 20 chords away from the wing geometry to allow the well development of the flow around the wing (Zhang *et al.* 2010).

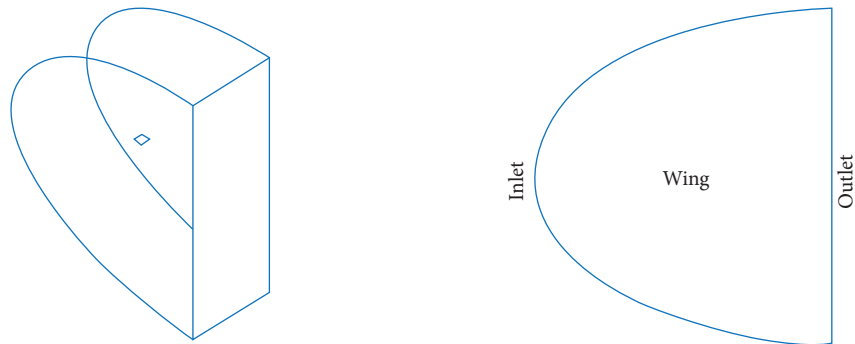


Figure 1. Fluid domain around the wing.

MESH

A fine mesh is one of the requirements to achieve accurate simulation results. The C-type grid topology is utilized in this research as it is found to be the efficient meshing method for wing geometry (Lei 2005). A fine mesh (Fig. 2) is achieved and implemented by defining edge sizing and inflation layers on the edge of the wing geometry and sweeping the achieved mesh along the wing span.

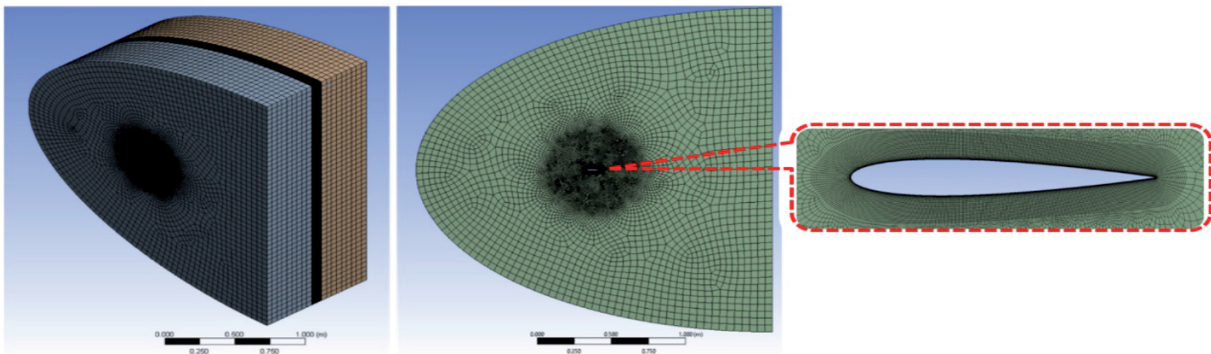


Figure 2. Mesh of the fluid domain.

To achieve the efficient mesh, different mesh edge sizing and inflation layers were generated and simulations were conducted with different cell numbers ranging from 60000 cells to 1.3 million cells. Based on the convergence time, achieved wall Y^+ and accuracy of the results obtained from simulations, the following geometry mesh characteristics are selected (Table 1):

Table 1. Mesh characteristics.

Mesh control	Location	Size
Entire fluid domain	Wing center	1×10^{-2}
Edge sizing	Wing edge (airfoil)	5×10^{-4}
Surface inflation	Fluid surface around the wing	1×10^{-5} (first cell height)

NUMERICAL SETUP

The flow is considered to be incompressible since the Mach number is less than 0.3. A pressure-based solver is selected. The properties of the fluid are presented in Table 2. The Spalart-Allmaras turbulence model is selected for the simulations as it was investigated by Lei (2005) and it is found to be the efficient and applicable turbulent model for wing simulations at low speeds.

Table 2. Simulation fluid properties assumptions.

Fluid properties			
Fluid	Temperature	Density (kg/m ³)	Viscosity (kg/ms)
Air	20°	1.225	1.7894×10^{-5}

EXPERIMENTAL

EXPERIMENTAL APPARATUS

The results obtained from simulations on the wing are validated by experimental results. The wing geometry is fabricated using Taylor's University 3D printing machine. The precision of the manufactured wing geometry is evaluated by comparing the model with printed technical drawing of the wing model prepared using Solidworks 15. The precisely evaluated wing models are installed in the Taylor's University low speed wind tunnel test section to conduct experiments. Taylor's University wind tunnel (TUWT) is an open subsonic wind tunnel model with 3:4:1 contraction ratio (Fig. 3). The test section of the wind tunnel is rectangular with a square cross section of 0.303 m × 0.303 m and length of 0.885 m. A Gamma DAQ F/T transducer is utilized to collect force and moment data. The force and moment readings from the transducer sensor are accurately measured and displayed using a PCI DAQ card model of NI PCI-6220 installed in the computer. The flow is created using a fan with a diameter of 0.63 m, 3 hp and 4145 V.50 Hz.

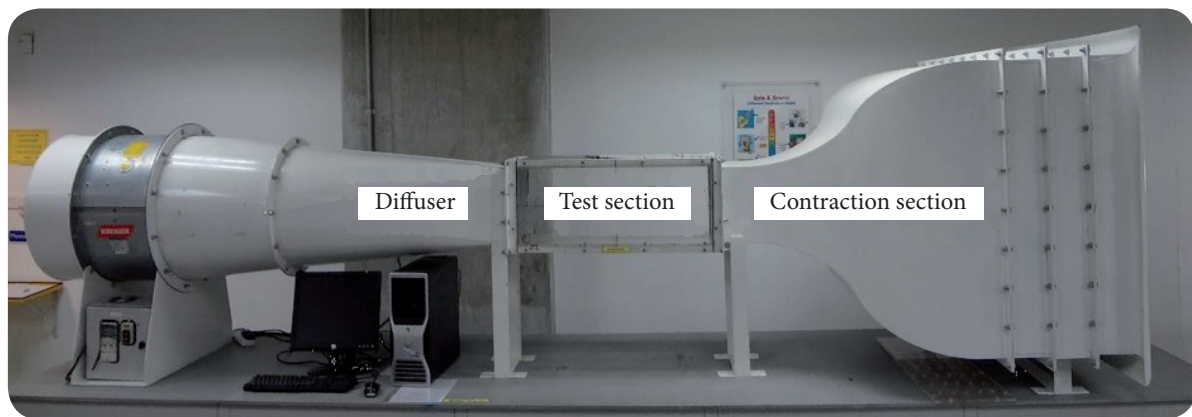


Figure 3. Taylor's University subsonic wind tunnel.

EXPERIMENTAL SETUP

A force measurement mechanism is designed, calibrated and installed on the Taylor's University wind tunnel prior to experiments conduction. The mechanism consists of the following components (Fig. 4):

1. Heavy base
2. Tool side fixture shaft
3. 6-axis transducer (GAMMA ATI)

4. Model mounting adaptor
5. Rotary mechanism
6. Model mounting strut
7. Base stand

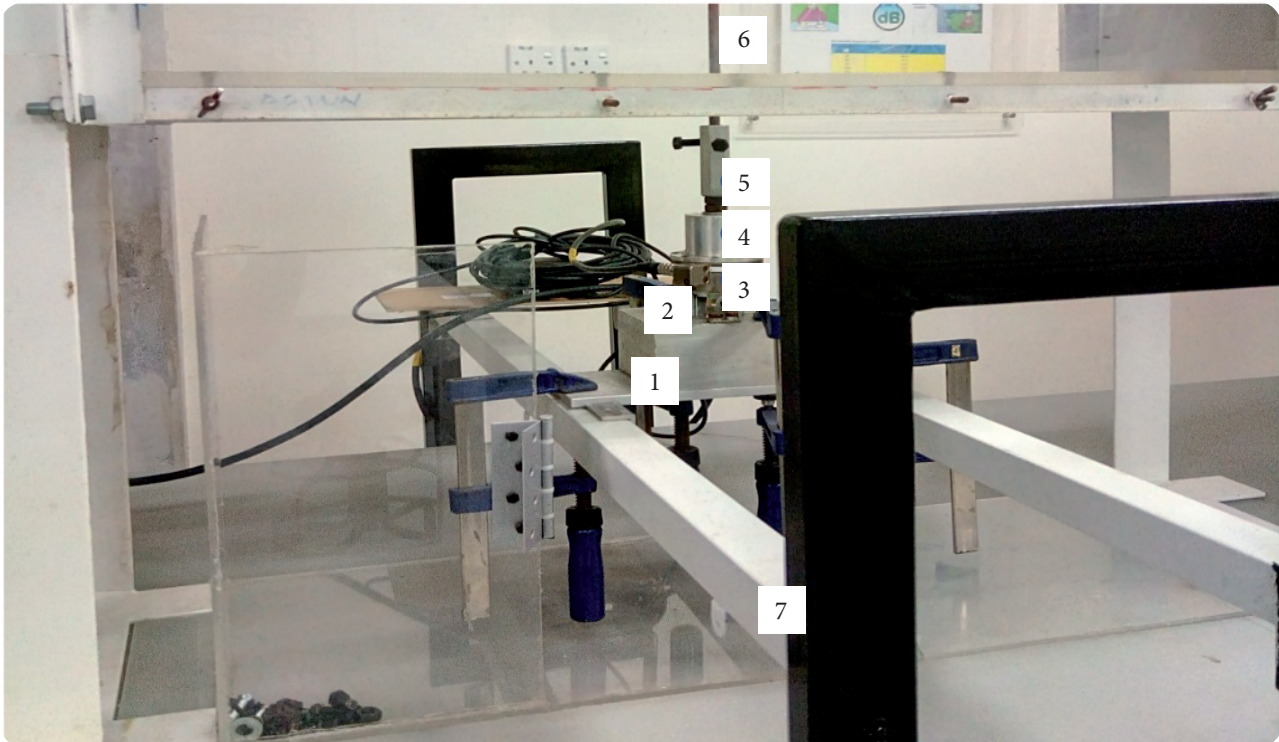


Figure 4. Force measurement mechanism.

The load cell is fixed on a base through its tool side as suggested in the load cell's technical manual. The aluminum fixture shaft is custom designed and manufactured utilizing CNC machine. The base is mounted on a stand fixed on the floor to avoid any vibration caused by the operation of wind tunnel. The custom model mounting geometry is manufactured and attached to the mounting adaptor plate. The model mounting part enables the installation of model struts on the load cell. The strut holds the wing model inside the wind tunnel test section and transfers the forces acting on the wing to the load cell. The load cell is connected to a DAQ system that collects the data and transfers it to a computer. The collected data will be shown in an excel sheet and various graphs for different aerodynamic characteristics, such as lift and drag forces, are plotted. In order to validate the experimental set up, experiments are conducted at different angle of attack on NACA0012 wing and the results obtained from the experiments are compared with experimental data publish by Chinwicharnam *et al.* (2015). The operating speed of the wind tunnel is adjusted to achieve the similarity. For physical similarity, Reynold's number (Re_c) has to be maintained the same as the published data. The operational speed is calculated using Eq. 1:

$$Re_c = \frac{\rho V l}{\mu} \quad (1)$$

where ρ and μ are the density and kinematic viscosity of air respectively, l is the chord length of the wing and V is the velocity of the flow.

WING MODEL

The experiments are conducted on the NACA0012 wing model with chord length of 0.15 m and aspect ratio of 1. The wing is installed through its aerodynamic center (Flandro *et al.* 2011). The aerodynamic center of the wing is calculated using Eq. 2:

$$AC = \frac{c}{4} \quad (2)$$

where AC is the aerodynamic center from the leading edge and C is the chord length of the wing, as shown in Fig. 5.

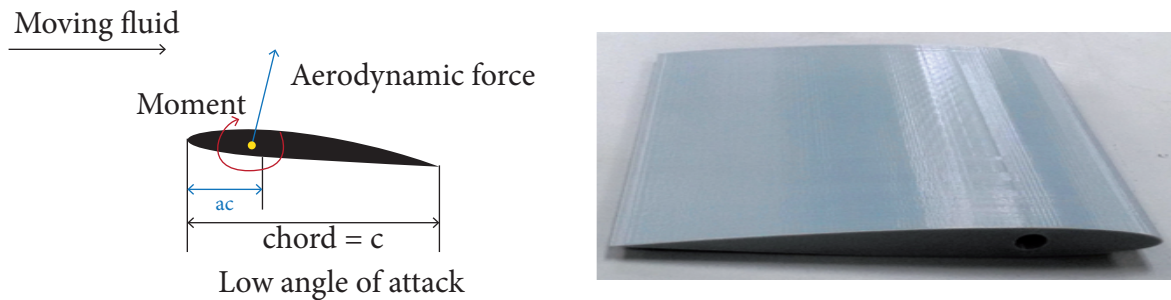


Figure 5. (a) Aerodynamic center of wing and (b) NACA0012 wing model.

RESULTS AND DISCUSSION

AERODYNAMIC CHARACTERISTICS AT DIFFERENT ANGLES OF ATTACK

The stream flow analysis provides a better understanding of the pressure distribution around the airfoil at different angle of attack. It is observed in Fig. 6 that the flow stream sticks to the airfoil surface at 0° angles of attack. As the angle of attack increases to 5° , the stream starts to separate from the airfoil's upper surface, and the separation moves towards the leading edge of airfoil by increasing the angle of attack. Separation of the flow from the airfoil results in the formation of eddies starting from where the flow is separated towards the trailing edge of the airfoil, as the flow tends to stick back to the airfoil's surface. Formation of eddies causes chaos, therefore the flow loses its laminar characteristics as since the flow path line is not predictable anymore. Increasing the angle of attack results in more separated region from the airfoil surface hence more turbulence. Figure 6 shows that the flow stream is symmetric at 0° angle of attack and the velocity of the upper and lower surface of the airfoil are equal, while increasing the angle of attack from 0° to 20° results in higher flow velocity on the upper surface compared to lower surface of the airfoil. Based on Bernoulli's principle, air flows at higher speed through regions with lower pressure. Therefore, it can be said that the pressure at the upper surface of the airfoil is less than the lower surface airfoil since the upper surface velocity is higher than the velocity at lower surface (Fig. 6). The pressure difference between the lower and upper body of the airfoil results in lift force, caused by increasing the angle of attack from 0° to 15° . This results in pressure increment on the lower surface of the airfoil, hence increment in lift force as the angle of attack increases.

The behavior of drag coefficient with respect to angle of attack at different Reynold's numbers is shown in Fig. 7. A positive gradient for drag coefficient is observed as the angle of attack is increased despite the change of Reynold's number. The drag coefficient is continuously increased as the angle of attack is increased to 74° with C_d of 0.72. However, the drag slope for angle of attack less than 20° is gentle, while drag slope is steeper as the angle of attack is increased to 74° . Further increment in the angle of attack from 74° to 82° results in slight linear reduction in the drag coefficient and eventually it stays constant for angle of attack ranging from 82° to 90° .

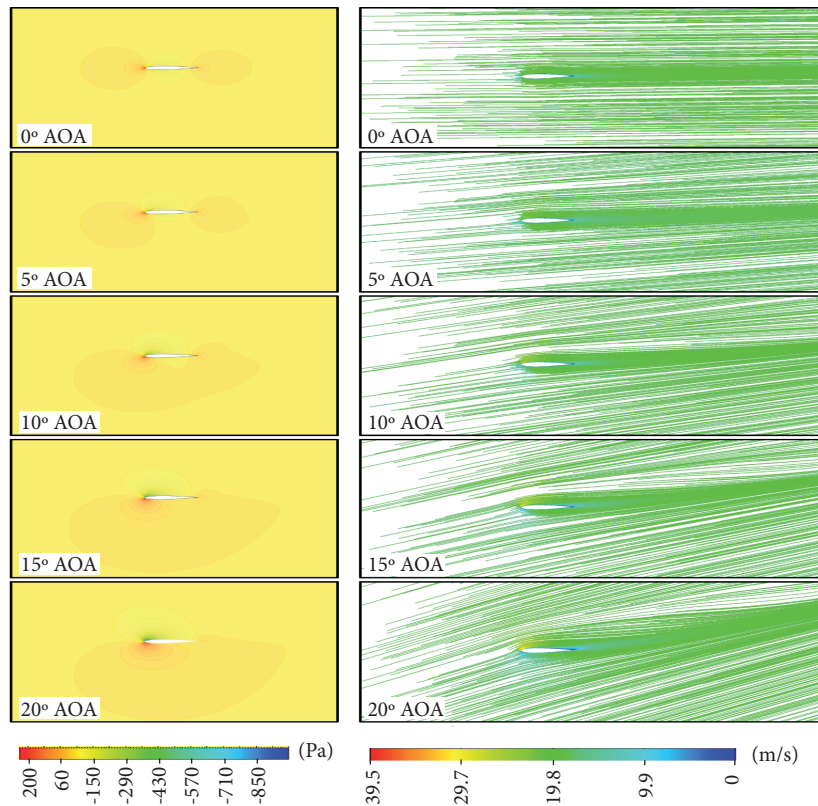


Figure 6. (a) Pressure contour and (b) velocity stream.

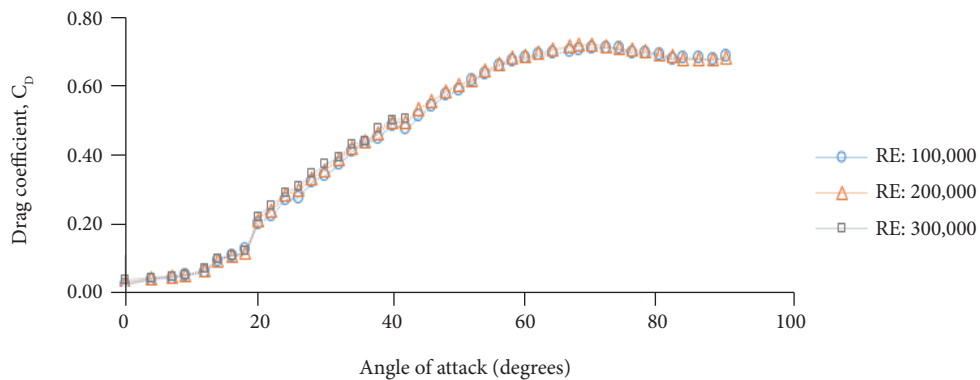


Figure 7. C_D vs. angle of attack.

Observation of lift coefficient at different angles of attack and Reynold's numbers (Fig. 8) shows that the lift coefficient is linearly increasing until it reaches its peak value at 32° angle of attack (stall angle) with C_L of 0.58, 0.63 and 0.65 at Re of 1×10^5 , 2×10^5 and 3×10^5 , respectively. Further increment of angle of attack results in continuous reduction in C_L until it reaches a value of 0.03 at 90° angle of attack. This can be explained by significant adverse pressure gradient at the leading edge of the airfoil, which results in separation of the flow and formation of vortices, consequently the wing experiences a low speed flow with high turbulence intensity on its upper surface. Thus, the pressure on the upper surface of the wing is increased, which results in decrement of the lift coefficient. The polar curve is shown in Fig. 9, which provides an overview of aerodynamic performance of NACA0012. Drag

coefficient is at its lowest for 0° angle of attack and it is increased as the angle of attack is increased to 90° , showing the highest amount of drag on the wing resulting in lowest lift coefficient. Comparisons of the aerodynamic characteristics of the wing at different low Reynold's number show similar trend, which suggests weak dependence of aerodynamic characteristics of wing on Re_c at low Reynold's number regime. This can be explained by the insignificant change in the laminar-turbulent transition location at different Re_c .

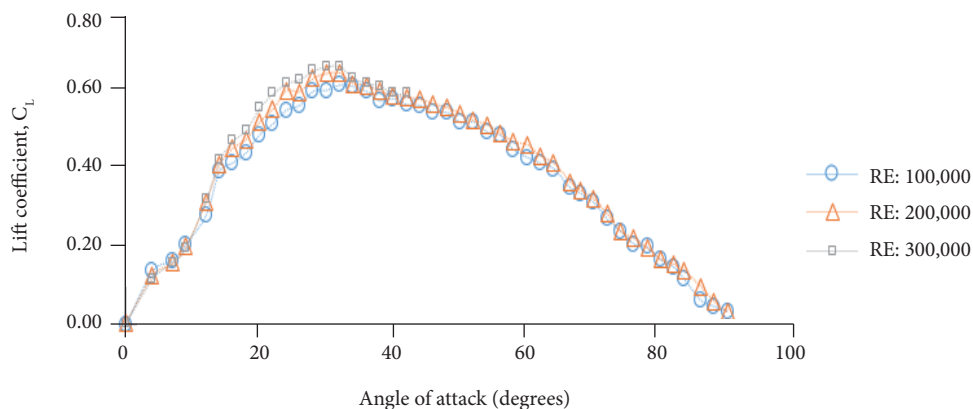


Figure 8. C_L vs. angle of attack.

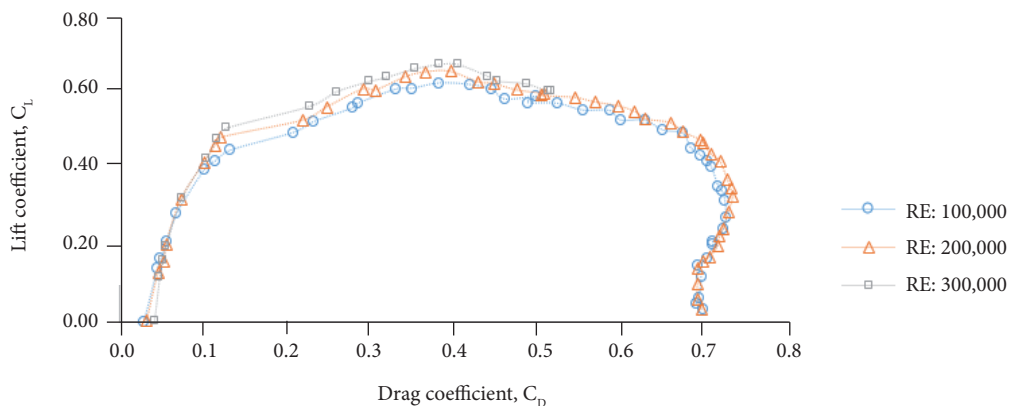


Figure 9. Drag polar at different Reynold's number.

VALIDATION OF RESULTS

The wind tunnel speed was set to 13.1 m/s to achieve Reynold's number of 1.29×10^5 . The lift and drag coefficients for 0° to 20° angle of attack obtained from the experiments are compared with the numerical results and available published results (Chinwicharnam et al. 2015) to evaluate the accuracy of the results obtained from numerical simulation and experiments as, shown in Figs. 10 and 11. The experimental results show that the largest percentage error of the lift and drag coefficients at 20° angle of attack are 13% and 14%. This error has occurred due to the sensitivity of the load cell to vibration of the test rig while the wind tunnel operates.

Comparison of the numerical results with the data obtained from wind tunnel experiments show that the lift and drag coefficients obtained from simulations complement the experimental results with minor error of 3% at angle of attack less than 15° . However, at 20° angle of attack, the simulation results differ from published experimental results by 19%, which is caused by increased

wall Y^+ at the leading edge of the wing (Fig. 12). This is caused by the flow separation at leading edge due to high angle of attack. Further refinement of the mesh around the wing's leading edge helps reducing the percentage obtained. However, the trends of the results obtained from the experiments are in complement with numerical results from the published experimental data.

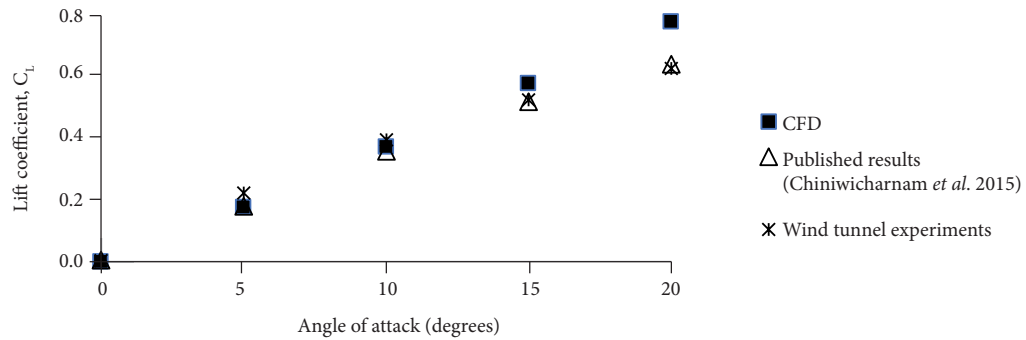


Figure 10. Validation of C_L .

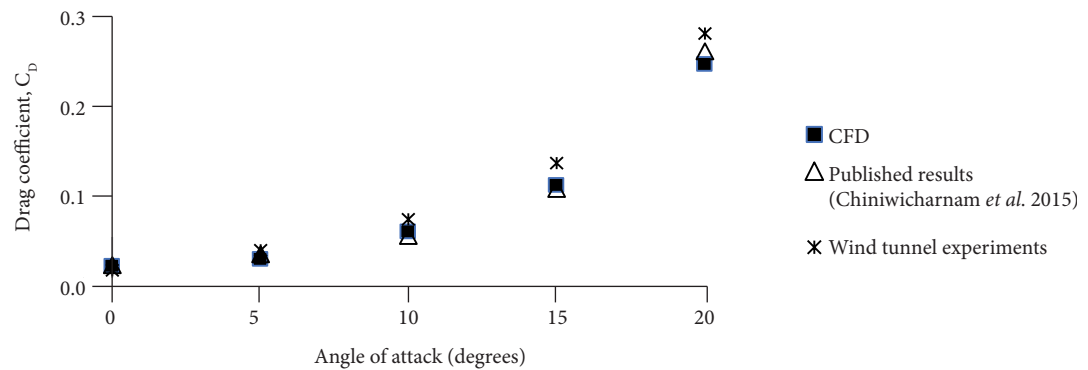


Figure 11. Validation of C_D .

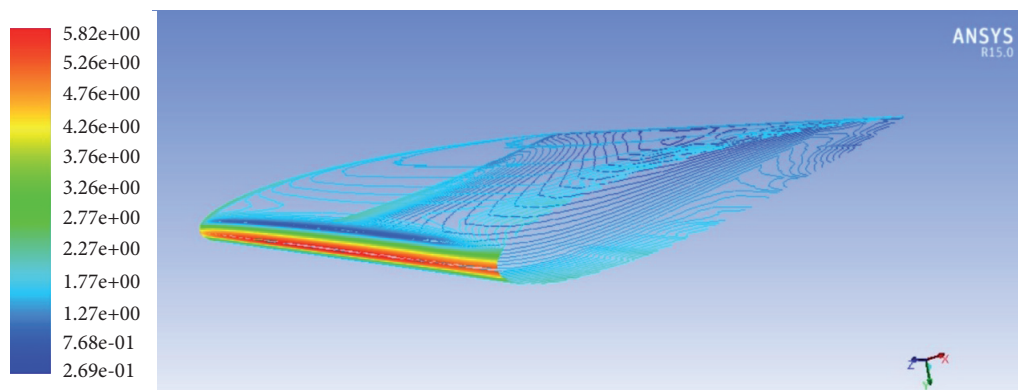


Figure 12. Wall Y^+ at 20° angle of attack.

CONCLUSION

In the present research, numerical and experimental studies are conducted on a NACA0012 finite wing geometry at different angles of attack and low Reynold's numbers. The findings of the research are summarized as below:

- The lift coefficient increases with increasing of angle of attack until 32°, where the lift reaches its maximum value and further increments of angle of attack decreases the lift coefficient until it reaches its minimum value at 90°, which can be explained by significant adverse pressure gradient at the leading edge of the airfoil that results in separation of the flow and formation of vortices; consequently, the wing experiences a low speed flow with high turbulence intensity on its upper surface. Thus, the pressure on the top of wing is increased, which causes the lift coefficient continuous decrement.
- The drag force acting on the airfoil increases as the angle of attack is increased and increment in the drag force results in change of laminar flow to turbulent flow. As the turbulence get higher, the flow starts to separate from the airfoil surface due to eddies generated by turbulence. Hence, the lift force generated by the wing is reduced and drag force is simultaneously increased, which results in poor performance of the wing.

AUTHORS' CONTRIBUTION

Conceptualization, Eftekhari S and Al-Obaidi ASM; Methodology, Eftekhari S and Al-Obaidi ASM; Investigation, Eftekhari S; Writing – Original Draft, Eftekhari S; Writing – Review and Editing, Eftekhari S and Al-Obaidi ASM; Funding Acquisition, Eftekhari S and Al-Obaidi ASM; Supervision, Al-Obaidi ASM.

FUNDING

School of Engineering, Taylor's University, Project "A cruising fixed wing mini-UAV: optimisation of aerodynamic and performance of civil applications".

Grant No: TRGS_MFS_2_2016_SOE_010

REFERENCES

- Abbott IH, Von Doenhoff AE (1959) Theory of wing sections: including a summary of airfoil data. New York: Dover Publications.
- Ahmed T, Amin MT, Islam SMR, Ahmed S (2014) Computational study of flow around a NACA 0012 wing flapped at different flap angles with varying Mach numbers. *Glob J Res Eng* 13(4):4-16.
- Chahl J (2015) Unmanned Aerial Systems (UAS) research opportunities. *Aerospace* 2(2): 189-202. <https://doi.org/10.3390/aerospace2020189>
- Chinwicharnam K, Ariza EDG, Moschetta J-M, Thipyopas C (2015) A computation study on the aerodynamic influence of interaction wing-propeller for a tilt-body MAV. *Aircr Eng Aerosp Technol An Int J* 87(6):521-529. <https://doi.org/10.1108/AEAT-06-2014-0087>
- Chung TJ (2002) Computational Fluid Dynamics. Cambridge: Cambridge University Press.
- Devinant P, Laverne T, Hureau J (2002) Experimental study of wind-turbine airfoil aerodynamics in high turbulence. *Journal of Wind Engineering and Industrial Aerodynamics* 90(6):689-707. [https://doi.org/10.1016/S0167-6105\(02\)00162-9](https://doi.org/10.1016/S0167-6105(02)00162-9)
- Lei Z (2005) Effect of RANS turbulence models on computation of vortical flow over wing-body configuration. *Trans Jpn Soc Aeronaut Space Sci* 48:152-160. <https://doi.org/10.2322/tjsass.48.152>
- Flandro GA, McMahon HM, Roach RL (2011) Basic aerodynamics: incompressible flow. Cambridge: Cambridge University Press.
- Kim D-H, Chang J-W, Chung J (2011) Low-Reynolds-Number effect on aerodynamic characteristics of a NACA 0012 airfoil. *J Aircr* 48(4):1212-1215. <https://doi.org/10.2514/1.0031223>

Windi IS, Faris MA, Kareem H (2014) Experimental and theoretical investigation for the improvement of the aerodynamic characteristic of NACA 0012 airfoil. International Journal of Mining, Metall Mech Eng 2(1):11-15.

Zhang Y, Huang Y, Wang F, Tan Z (2010) Numerical simulation of the airfoil flowfields at angles of attack from 0° and 180°. Presented at: Asia-Pacific Power and Energy Engineering Conference; Chengdu, China. <https://doi.org/10.1109/APPEEC.2010.5448906>

Zhou Y, Alam MM, Yang HX, Guo H, Wood DH (2011) Fluid forces on a very low Reynolds number airfoil and their prediction. International Journal of Heat Fluid Flow 32(1):329-339. <https://doi.org/10.1016/j.ijheatfluidflow.2010.07.008>